on any particular stretch of DNA is entropically expensive and thus statistically unlikely, unless there is a compensating stabilization resulting from the binding of a histone octamer to this particular DNA sequence. Cooperation from other favorable contributions could aid positioning by lowering the specific histone–DNA binding energy requirement. For example, as may occur on the 35S gene, a stretch of inaccessible DNA, covered by specific (regulatory?) proteins, could effectively direct nucleosomes to the first available DNA, immediately adjacent to the protected domain. From a first nucleosome, regularity could be maintained by the forces which determine internucleosomal locations, forces which seem able to compensate for the unfavorable entropy of specific locations. However, since these forces probably do not specify unique internucleosomal locations (Lohr & Van Holde, 1979), the initial precise positioning could degenerate downstream.

Registry No. Staphylococcal nuclease, 9013-53-0; DNase I, 9003-98-9.

References

Alwine, J., Kemp, P., Parker, B., Reiser, J., Renart, J., Stark, G., & Wahl, G. (1979) *Methods Enzymol. 68*, 220–242.

Bayev, A., Georgiev, O., Hadjiolov, A., Kermekchiev, A., Nikolaev, N., Skyrabin, D., & Sakharyev, V. (1980) *Nucleic Acids Res. 8*, 4919–4926.

Bloom, K., & Carbon, J. (1982) *Cell (Cambridge, Mass.) 29*, 305–317.

Cartwright, I., & Elgin, S. C. (1982) *Nucleic Acids Res. 10*, 5835–5852.

Dingwall, C., Lomonossoff, G., & Laskey, K. A. (1981) *Nucleic Acids Res. 9*, 2659–2673.

Goodman, H. (1980) *Methods Enzymol. 65*, 63–64.

Horz, W., & Altenburger, W. (1981) *Nucleic Acids Res. 9*, 2643–2658.

Igo-Kemenes, T., Horz, W., & Zachau, H. (1982) *Annu. Rev. Biochem. 51*, 89–123.

Klemenz, R., & Geiduschek, P. (1980) *Nucleic Acids Res. 8*, 2679–2684.

Levy, A., & Noll, M. (1979) *Nucleic Acids Res. 8*, 6059–6068.

Lohr, D. (1983) *Biochemistry 22*, 927–935.

Lohr, D., & Ide, G. (1979) *Nucleic Acids Res. 6*, 1909–1927.

Lohr, D., & Van Holde, K. (1979) *Proc. Natl. Acad. Sci. U.S.A. 76*, 6326–6330.

Lohr, D., Kovacic, R. T., & Van Holde, K. E. (1977a) *Biochemistry 16*, 463–471.

Lohr, D., Tatchell, K., & Van Holde, K. (1977b) *Cell (Cambridge, Mass.) 17*, 829–836.

Lutter, L. (1978) *Cold Spring Harbor Symp. Quant. Biol. 42*, 137–147.

Lutter, L. (1979) *Nucleic Acids Res. 6*, 41–56.

Maxam, A., & Gilbert, W. (1980) *Methods Enzymol. 65*, 499–560.

McGhee, J., & Felsenfeld, G. (1980) *Annu. Rev. Biochem. 49*, 1115–1156.

McGhee, J., & Felsenfeld, G. (1983) *Cell (Cambridge, Mass.) 32*, 1205–1215.

Noll, M. (1977) *J. Mol. Biol. 116*, 49–71.

Reeder, R., Wilkinson, J., Bakken, A., Morgan, G., Busby, S., Roan, J., & Sollner-Webb, B. (1983) *Cold Spring Harbor Symp. Quant. Biol. 47*, 867–871.

Stellwag, E., & Dahlberg, A. (1980) *Nucleic Acids Res. 8*, 299–317.

Von Hippel, P., & Felsenfeld, G. (1964) *Biochemistry 3*, 27–39.

Resonance Raman Detection of Fe–CO Stretching and Fe–C–O Bending Vibrations in Sterically Hindered Carbonmonoxy "Strapped Hemes". A Structural Probe of Fe–C–O Distortion†

Nai-Teng Yu,* Ellen A. Kerr, Brian Ward, and C. K. Chang*

ABSTRACT: We report resonance Raman studies of the Fe–C–O distortion in sterically hindered heme–CO complexes. The steric hindrance is provided by a hydrocarbon chain strapped across one face of the heme. Increasing the steric hindrance (by decreasing the chain length), which reduces the CO binding affinity, is found to increase the Fe–CO stretching frequencies: heme 5 (unstrapped), 495 cm^{-1}; FeSP-15, 509 cm^{-1}; FeSP-14, 512 cm^{-1}; FeSP-13, 514 cm^{-1}. This is interpreted in terms of a decrease in the CO effective mass and increased interactions between the C atom of CO and the N atom(s) of the pyrrole ring(s). Resonance Raman enhancement of the Fe–C–O bending mode upon Soret excitation may be correlated with the overlap between the porphyrin (π^*) and CO (π^*) orbitals when the CO ligand is tilted. Its intensity relative to that of the Fe–CO stretching mode increases with increasing steric hindrance in these "strapped hemes". In addition, we have estimated the Fe–C–O angles from isotope data in various heme–CO complexes. It is inferred that the angles are 167 ± 5° (FeSP-15) and 175 ± 5° (FeSP-14, FeSP-13, Mb·CO, and Hb·CO).

The steric hindrance by distal residues in hemoproteins plays an important role in the regulation of heme reactivity toward different ligands (Moffat et al., 1970, and references cited therein; Szabo, 1978). The heme pockets of biological oxygen carriers such as hemoglobins (Hb) and myoglobins (Mb) have a geometry that fits dioxygen (O_2) in its natural bent, end-on configuration (Collman et al., 1974; Phillips, 1978, 1980; Shaanan, 1982) but not a carbon monoxide (CO) molecule, which preferentially binds to the iron in a linear and perpendicular fashion (Hoard, 1975; Peng & Ibers, 1976). It has been proposed that the distal steric effect lowers the affinity

† From the School of Chemistry, Georgia Institute of Technology, Atlanta, Georgia 30332 (N.-T.Y. and E.A.K.), and the Department of Chemistry, Michigan State University, East Lansing, Michigan 48824 (B.W. and C.K.C.). *Received January 4, 1983.* This work was supported by National Institutes of Health Grant GM 18894 and National Science Foundation Grant CHE-8210200. C.K.C. is an Alfred P. Sloan Fellow (1980–1984) and a Camile Henry Dreyfus Teacher–Scholar (1980–1985).

0006-2960/83/0422-4534$01.50/0

ratio of CO vs. O_2 and is responsible for the partial detoxification of CO in respiratory organisms (Caughey, 1970; Perutz, 1976; Collman et al., 1976, 1979). In fact, X-ray diffraction studies of several carbonmonoxy-Hb's and -Mb's have revealed a distorted Fe–C–O linkage with respect to the porphyrin ring (Huber et al., 1970; Heidner et al., 1976; Baldwin, 1980; Norvell et al., 1975; Steigemann & Weber, 1979; Padlan & Love, 1975). The oxygen atom of the carbonyl is definitely displaced off the heme axis, but there are still some questions concerning the detailed geometry of the Fe–C–O linkage in carbonmonoxy hemoproteins.

Resonance Raman spectroscopy is ideally suited for investigating the nature of the Fe–C–O distortion; important structural information is contained in the three normal vibrations associated with the Fe–C–O linkage, which are now detectable with Soret excitation (Tsubaki et al., 1982). Since numerous factors can affect the vibrational frequencies, a systematic study on the effects of each factor employing model compounds is essential before reliable structural correlations can be established.

Here we report a study of the distal steric effect on the Fe–CO stretching, Fe–C–O bending, and C–O stretching vibrations. Four synthetic hemes (with *N*-methylimidazole as a base) were employed: a simple iron porphyrin (heme 5) without groups to hinder the CO binding and three "strapped hemes", which have a 13-, 14-, or 15-atom hydrocarbon strap across the CO binding site (Ward et al., 1981). It was found that when the chain length was decreased (hence, increasing the steric hindrance or decreasing the CO binding affinity), the Fe–CO stretching frequency increases but the C–O stretching frequency decreases. We demonstrate that while the Fe–C–O bending mode is not detectable in heme 5, its intensity relative to that of the Fe–CO stretching mode increases in the order FeSP-15 < FeSP-14 < FeSP-13; the CO distortion causes the enhancement of the Fe–C–O bending mode. These spectral features are interpreted in terms of increased interactions between the CO ligand and the N atom(s) of the pyrrole ring(s) in both ground and excited states. To estimate the Fe–C–O bond angles, we have employed a simple equation that requires only two stretching frequencies for two different isotopes without a prior knowledge of force constants.

Materials and Methods

The strapped hemes (FeSP-13, FeSP-14, and FeSP-15) and heme 5 (Figure 1) were synthesized by the method described previously (Ward et al., 1981). Pyrrole ^{15}N substituted iron(III) tetraphenylporphyrin chloride (FeTPPCl) was synthesized from [^{15}N]pyrrole (Merck & Co., 95 atom % ^{15}N) and benzaldehyde in propionic acid with a standard procedure (Kim et al., 1978). The CO complexes of these hemes were prepared with *N*-methylimidazole (N-MeIm) as the axial base in benzene solution (containing 10% CH_2Cl_2 to increase solubility) at room temperature. The sample solution (1 mL, 100 μM heme and 500 μM base) was placed into a cylindrical quartz Raman cell. The reduction was carried out by the addition of a minimum amount of a reducing solution prepared by the 10-fold dilution with benzene of Vitride T reducing agent (J. T. Baker Chemical Co., 70% $C_6H_{16}AlNaO_4$ in toluene). The cell was immediately sealed with a rubber septum and evacuated. Carbon monoxide ($\sim$1 atm) was then introduced into the sample. The isotope-substituted complexes were prepared similarly with $^{13}C^{16}O$ (Prochem, 95 atom % ^{13}C), $^{13}C^{18}O$ (Prochem, 91.7 atom % ^{13}C and 98.5 atom % ^{18}O), and $^{12}C^{18}O$ (Stohler Isotope Chemicals, 99 atom % ^{18}O), each at an initial pressure of 1 atm.

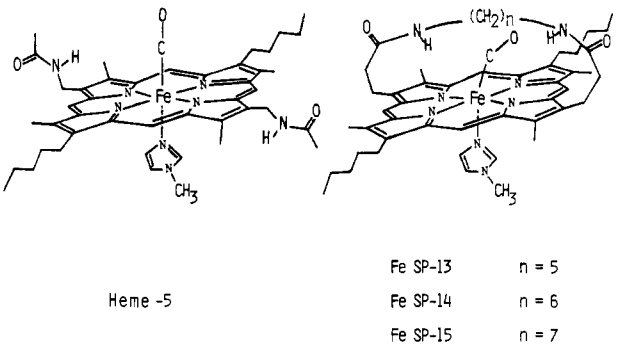

FIGURE 1: Chemical structures of heme 5 and strapped hemes.

All reagents were purified immediately prior to use. Benzene and methylene chloride were stirred over concentrated sulfuric acid to remove organic impurities, neutralized with a dilute $NaHCO_3$ solution, and dried over anhydrous $MgSO_4$. The solvents were distilled and stored under N_2: benzene from sodium benzophenone ketyl and methylene chloride from phosphorus pentoxide. *N*-Methylimidazole was distilled from KOH.

All Raman spectra were obtained with a highly sensitive multichannel laser Raman system (Yu & Srivastava, 1981), which consists of a dry ice cooled silicon-intensified target (SIT) detector (500 channels, 12.5-mm width), a detector controller, a microprocessor-based OMA2 console (PAR 1215), and a Spex 1402 0.85-m Czerny-Turner double-grating spectrometer. A Spectra-Physics Model 171-01 krypton laser was employed for excitation at 406.7 nm with laser power approximately 10 mW at the sample. The sample in the rotating Raman cell was spun throughout the measurements to avoid local heating and to lessen photodissociation. Scattered light was collected by a 90° geometry and the slit was 100 μm in width and 0.2 cm^{-1} in height. Fenchone was used to calibrate all spectra, and wavenumbers reported are accurate to ± 1 cm^{-1} for sharp lines and ± 2 cm^{-1} for broad lines.

Infrared measurements of the C–O stretching frequencies were carried out by using a Perkin-Elmer 283B spectrometer interfaced with a computer. The medium used was 0.1 M *N*-methylimidazole in CH_2Cl_2. Both infrared and resonance Raman measurements were performed at room temperature.

Results

Figure 1 shows the chemical structures of heme 5, FeSP-13, FeSP-14, and FeSP-15 (with CO ligand and N-MeIm base). In Figure 2, we compare resonance Raman spectra of these compounds (in oxidized form) in the 1300–1700-cm^{-1} region where the porphyrin ring vibrations appear. The π-electron density sensitive line (at $\sim$1372 cm^{-1}) (Rousseau & Ondrias, 1983, and references cited therein) and "core-size" indicator lines (1495, 1586, and 1631 cm^{-1}) (Spaulding et al., 1975; Spiro et al., 1979; Callahan & Babcock, 1981; Choi et al., 1982) are nearly the same, indicating that the electronic structure and heme geometry have not been modified by the straps. Figure 3 presents low-frequency resonance Raman spectra (100–700 cm^{-1}) of the $^{12}C^{16}O$, $^{13}C^{16}O$, $^{12}C^{18}O$, and $^{13}C^{18}O$ complexes of Fe^{II}(heme 5)(N-MeIm) excited at 406.7 nm. The only isotope-sensitive line at 495 cm^{-1} shifts to 491 ($^{13}C^{16}O$), 486 ($^{12}C^{18}O$), and 484 cm^{-1} ($^{13}C^{18}O$). The monotonous decrease in frequency as the CO mass increases from 28 to 31 daltons clearly indicates that it is the Fe–CO stretching vibration. The same vibration has been identified previously at 507 cm^{-1} in HbA·CO and 512 cm^{-1} in Mb·CO (Tsubaki et al., 1982) and at 505 cm^{-1} in carbonmonoxy

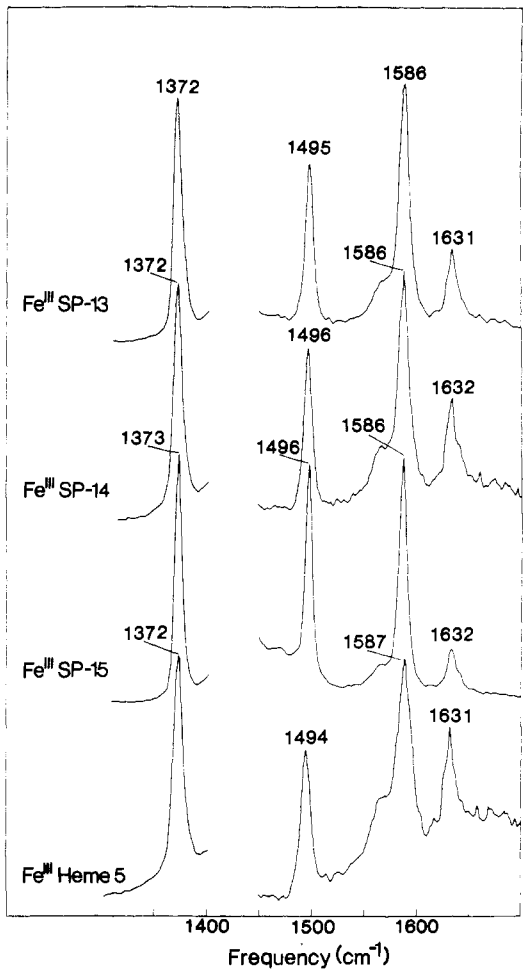

FIGURE 2: Resonance Raman spectra of strapped and unstrapped hemes (in oxidized form) in the 1300–1700-cm^{-1} region. λ_{ex} = 406.7 nm; concentration = 100 μM in methylene chloride. The solvent (CH_2Cl_2) peak at 1423 cm^{-1} has been omitted.

leghemoglobin (Armstrong et al., 1982; Rousseau et al., 1983). In contrast, the Fe–C–O bending mode, δ(Fe–C–O), is expected to exhibit a "zigzag" isotope shift pattern from $^{12}C^{16}O$ to $^{13}C^{18}O$ in the order of increasing mass, a direct consequence of the fact that carbon rather than oxygen binds directly to the much heavier iron. This bending mode has been reported at ~577 cm^{-1} in both Mb·CO and HbA·CO (Tsubaki et al., 1982) and at 436 and 519 cm^{-1} in a non-heme Fe–CO system (Kroeker et al., 1980). Careful examination on both sides of the $\tilde{\nu}_1$(Fe–CO) line at 495 cm^{-1} reveals no δ(Fe–C–O) bending mode. The CO complexes of other unhindered hemes such as Fe^{II}("picket-fence" porphyrin)(N-MeIm) and Fe^{II}TPP(Py) in benzene also exhibit no detectable δ(Fe–C–O) bending vibration with Soret excitation (Kerr et al., 1983).

Figure 4 presents resonance Raman spectra of the $^{12}C^{16}O$, $^{13}C^{16}O$, $^{12}C^{18}O$, and $^{13}C^{18}O$ complexes of Fe^{II}(SP-14)(N-MeIm). Perhaps the most interesting observation is the enhancement of the δ(Fe–C–O) bending vibration at 578 cm^{-1}. It does display a zigzag isotope shift pattern (578 → 563 → 575 → 561 cm^{-1}) expected of a bending mode. The intensity of this line in the $^{12}C^{16}O$ and $^{12}C^{18}O$ complexes is somewhat greater than that in the $^{13}C^{16}O$ and $^{13}C^{18}O$ complexes because of its accidental degeneracy with a porphyrin ring mode at ~575 cm^{-1}, the intensity of which is slightly enhanced by the perturbation (Tsubaki et al., 1982).

The Fe–CO stretching mode in Fe^{II}(SP-14)(N-MeIm)CO was detected at 504 and 512 cm^{-1}; the former shifts to 501 ($^{13}C^{16}O$), 497 ($^{12}C^{18}O$), and 495 cm^{-1} ($^{13}C^{18}O$), and the latter

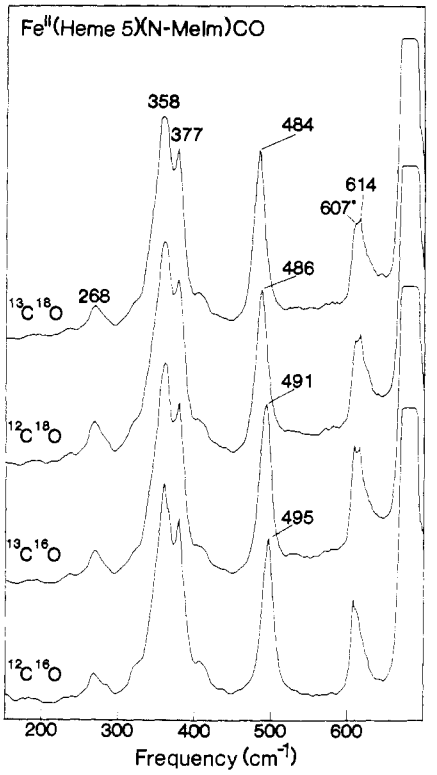

FIGURE 3: Effects of isotopic substitution on Fe–CO stretching in resonance Raman spectra of carbonmonoxy-Fe^{II}(heme 5)(N-MeIm) in the 100–70-cm^{-1} region. λ_{ex} = 406.7 nm; concentration = 100 μM in 10% methylene chloride in benzene. (*) Benzene line.

shifts to 508 ($^{13}C^{16}O$), 507 ($^{12}O^{18}O$), and 505 cm^{-1} ($^{13}C^{18}O$). Some variations in relative intensity have been noted. Under the same conditions, the unligated species exhibit no Raman lines at 504 or 512 cm^{-1}. Since our titration experiments monitored by optical absorption do indicate that N-MeIm is capable of binding to both "hindered" and "unhindered" sides in FeSP-14 (also in FeSP-15), the two $\tilde{\nu}_1$(Fe–CO) frequencies at 504 and 512 cm^{-1} (Figure 4) may correspond to linear CO (with N-MeIm on the strap side) and distorted CO (with N-MeIm on the unhindered side), respectively. The slightly higher $\tilde{\nu}_1$(Fe–CO) frequency at 504 cm^{-1} for the linear CO, compared to the 495-cm^{-1} value in heme 5 (Figure 3), is attributed to the weaker bonding between iron and N-MeIm on the strap side. It has been generally observed that the $\tilde{\nu}_1$(Fe–CO) frequency increases slightly as the trans iron–N_ϵ(Im) bond is weakened (Tsubaki et al., 1982; Kerr et al., 1982). In the Fe^{II}(SP-15)(N-MeIm)CO complex, the $\tilde{\nu}_1$(Fe–CO) vibration for the distorted CO was detected at 509 cm^{-1}. The shoulder at ~505 cm^{-1} may be due to the linear CO (with N-MeIm on the unhindered side). However, in the case of FeSP-13 (Figure 5), we still observed the doubling of the Fe–CO mode (506 and 514 cm^{-1}) even though the N-MeIm base does not bind to the strap side (Ward et al., 1981). It is possible that one of the species is a pentacoordinate CO complex with CO bound to the unhindered side. However, the $\tilde{\nu}_1$(Fe–CO) mode for a pentacoordinate CO complex normally appears at ~525 cm^{-1} (Kerr et al., 1983), which is much higher than the observed values (506 and 514 cm^{-1}). The alternative explanation is that for both components the CO is on the strap side but adopts different conformational states, resulting in more than one frequency for the Fe–CO stretching mode.

Comparison of Figures 3–5 reveals that the $\tilde{\nu}_1$(Fe–CO) frequency appears to increase in the order heme 5 < FeSP-15 < FeSP-14 < FeSP-13. In other words, the frequency of

Table I: Estimation of Fe–C–O Angles in Heme–CO Complexes[a]

compd	$\tilde{\nu}_1$ (cm^{-1})	$\tilde{\nu}_{1i}$ (cm^{-1})	$\tilde{\nu}_2$[e] (cm^{-1})	$\tilde{\nu}_{2i}$[e] (cm^{-1})	$P_{1/2}$(CO)[d] (torr)	∠FeCO[g] (deg)	tilt angle[b]	I_δ/I_ν[f]
heme 5	495	491	1954	1910	~2 × 10^{-4}	180	0	0
FeSP-15	509	503	1945	1901	5 × 10^{-2}	167 ± 5	+	0.10
FeSP-14	512	508	1939	1894	5 × 10^{-1}	175 ± 5	++	0.16
FeSP-13	514	510	1932	1888	12	175 ± 5	+++	0.25
Mb·CO[c]	512	509	1944	1896	~2 × 10^{-2}	175 ± 5		0.25
Hb·CO[c]	507	503	1951	1908	~4 × 10^{-3}	175 ± 5		0.10

[a] $\tilde{\nu}_1$, $\tilde{\nu}_{1i}$, $\tilde{\nu}_2$, and $\tilde{\nu}_{2i}$ are stretching frequencies (cm^{-1}) of Fe–CO, Fe–^{13}CO, C–O, and ^{13}C–O, respectively. [b] Angle between Fe–C and heme normal. 0 denotes a tilt angle of zero degree; increasing number of plus signs indicates increasing tilt angle. [c] Stretching frequencies taken from Tsubaki et al. (1982). [d] Data taken from Ward et al. (1981) and Collman et al. (1979). [e] $\tilde{\nu}_2$ and $\tilde{\nu}_{2i}$ for heme 5, FeSP-15, FeSP-14, and FeSP-13 were obtained in CH_2Cl_2 solution (0.1 M N-MeIm) by infrared spectroscopy. Measurements of these frequencies by resonance Raman were not successful because of fluorescence problems. [f] Intensity ratio between δ(Fe–C–O) bending and ν(Fe–CO) stretching vibrations. [g] In the calculations, we have used m_1 = 55.9, m_2 = 12.0, m_{2i} = 13.0, and m_3 = 16.0 amu. The effective iron mass due to its other bonds may be larger than the 55.9 value. The use of another value for m_1 will require a different calibration for $\theta = 180°$. When the angle is very close to 180°, the uncertainty is large.

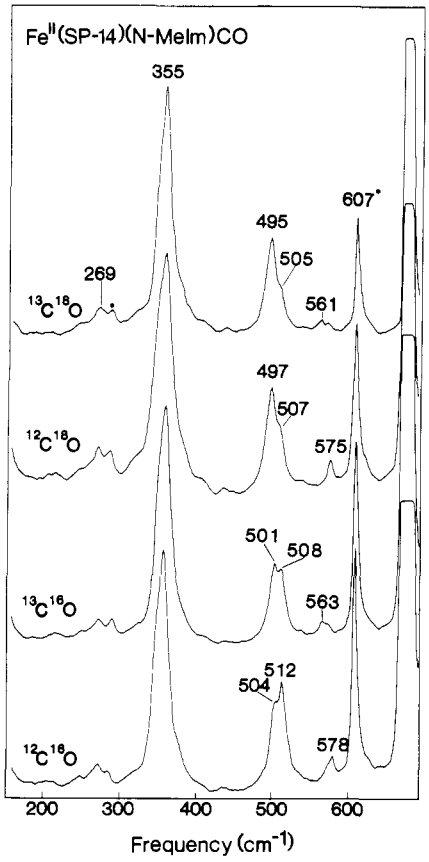

FIGURE 4: Effects of isotopic substitution on both Fe–CO stretching and Fe–C–O bending vibrations in resonance Raman spectra of carbonmonoxy-Fe^{II}(SP-14)(N-MeIm) in the 100–700-cm^{-1} region. λ_{ex} = 406.7 nm; concentrations = 100 μM in 10% methylene chloride in benzene. (*) Solvent lines.

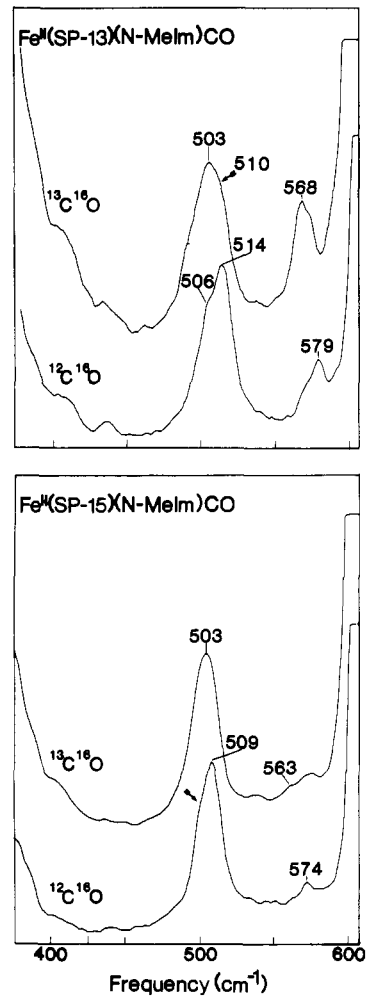

FIGURE 5: Resonance Raman spectra of carbonmonoxy-Fe^{II}(SP-13)(N-MeIm) (upper panel) and carbonmonoxy-Fe^{II}(SP-15)(N-MeIm) showing details of Fe–CO stretching and Fe–C–O bending vibrations as affected by $^{13}C^{16}O$ isotope substitution. λ_{ex} = 406.7 nm; concentration = 100 μM in 10% methylene chloride in benzene.

$\tilde{\nu}_1$(Fe–CO) increases with decreasing CO binding affinity (or increasing steric hindrance). This seemingly paradoxical correlation has also been found in oxy cobalt- and carbonmonoxy iron–picket-fence porphyrin complexes when N-MeIm (axial base) is replaced by 1,2-Me$_2$Im to decrease the binding affinity (Mackin et al., 1983; Kerr et al., 1982). In contrast, the C–O stretching frequency decreases (1954 → 1945 → 1939 → 1932 cm^{-1}) with decreasing CO binding affinity (see Table I). For the FeSP-13–CO complex, we detected a weak shoulder in the infrared C–O stretching region at ~1940 cm^{-1}, which presumably corresponds to the Fe–CO stretching frequency at 506 cm^{-1} (Figure 5); the 514-cm^{-1} line corresponds to the major CO stretching mode at 1932 cm^{-1}. In general, the $\tilde{\nu}_1$(Fe–CO) frequency increases with a decrease in $\tilde{\nu}_2$(C–O) (Kerr et al., 1983). However, for the CO complexes of FeSP-14 and FeSP-15, we have not resolved the splitting of the CO stretching mode.

A striking feature between the two panels in Figure 5 is the difference in the intensity of δ(Fe–C–O) relative to that of $\tilde{\nu}_1$(Fe–CO). In the spectrum of Fe^{II}(SP-13)(N-MeIm)CO, the δ(Fe–C–O) mode at 579 cm^{-1} is considerably stronger than that at 574 cm^{-1} in Fe^{II}(SP-15)(N-MeIm)CO. Taking into account the overlap with a porphyrin ring mode at 575 cm^{-1}

and the presence of two $\tilde{\nu}_1$(Fe–CO) frequencies, one may roughly estimate the intensity ratios, I_δ/I_ν, for the distorted Fe–C–O linkages as 0.10 (FeSP-15), 0.16 (FeSP-14), and 0.25 (FeSP-13). Here we assume that the species with a linear CO on the unhindered side contribute no intensity to the δ(Fe–C–O) line. It therefore appears that this intensity ratio increases with increasing steric hindrance (or geometric distortion).

To estimate the Fe–C–O angles in various heme–CO complexes, we have employed an equation (see Discussion) that requires only two stretching frequencies for two different isotopes. The results of our estimation for strapped hemes, Mb·CO, and HbA·CO are tabulated in Table I, along with data for $\tilde{\nu}_1$(Fe–CO), $\tilde{\nu}_{1i}$(Fe–^{13}CO), $\tilde{\nu}_2$(C–O), $\tilde{\nu}_{2i}$(^{13}C–O), $P_{1/2}$(CO) and I_δ/I_ν.

Discussion

Estimation of Fe–C–O Bond Angles in Heme–CO Complexes. The stretching frequencies, either $\tilde{\nu}_1$(Fe–CO) or $\tilde{\nu}_2$(C–O), may be influenced by numerous factors (Kerr et al., 1982; Alben & Caughey, 1968; Barlow et al., 1976; Traylor, 1981) that affect σ-electron donation and π-back-bonding. Thus, these frequencies per se sometimes are not reliable indicators of the Fe–C–O geometry. However, the data of isotopic shifts involving these two frequencies may be employed to estimate the Fe–C–O angles, as will be discussed here. To a first approximation, the Fe–C–O linkage may be treated as an isolated three-body oscillator. The stretching vibrations of the Fe–C–O linkage are not expected to couple significantly to the in-plane porphyrin ring modes because they are orthogonal. In this study, we demonstrate that the $\tilde{\nu}_1$(Fe–CO) frequency at 489 cm^{-1} in Fe^{II}TPP(N-MeIm)CO is insensitive (within ±1 cm^{-1}) to the pyrrole ^{14}N → ^{15}N substitution. However, there may be some weak couplings with the trans Fe–Im linkage (Tsubaki et al., 1982). These are neglected until a more sophisticated method is developed.

Recently, Champion et al. (1982) employed a three-body oscillator model to estimate the Fe–S–C angle in cytochrome P-450 (camphor), employing two isotope shifts. Our approach here combines their equations to eliminate the force constants so that the Fe–C–O angle may be estimated from isotope shifts without knowing the force constants or their ratios.

The Fe–C–O bending force constants (~0.5 mdyn/Å) are generally much smaller than the stretching force constants for Fe–C (~2.85 mdyn/Å) and C–O (~15.8 mdyn/Å) (Tsubaki et al., 1982) and thus may be neglected. The expressions for the two stretching vibrations ($\tilde{\nu}_1$ for Fe–CO; $\tilde{\nu}_2$ for C–O) may then be given by (Wilson, 1939; Champion et al., 1982):

$$\lambda_{1,2} = \frac{1}{2}\left(\frac{k_1}{\mu_1} + \frac{k_2}{\mu_2}\right) \pm \frac{1}{2}\left[\left(\frac{k_1}{\mu_1} + \frac{k_2}{\mu_2}\right)^2 - 4k_1k_2\left(\frac{1}{M^2} + \frac{\sin^2\theta}{m_2^2}\right)\right]^{1/2}$$

where $\lambda_1 = 4\pi^2(c\tilde{\nu}_1)^2$, $\lambda_2 = 4\pi^2(c\tilde{\nu}_2)^2$, c = speed of light, k_1 and k_2 = bond stretching force constants for Fe–C and C–O, respectively, $\mu_1 = m_1m_2/(m_1 + m_2)$, $\mu_2 = m_2m_3/(m_2 + m_3)$, $M^2 = m_1m_2m_3/(m_1 + m_2 + m_3)$, and m_1, m_2, and m_3 are masses for Fe, C, and O, respectively. The minus sign is for λ_1 and the plus sign for λ_2. For different isotopes, λ_1 and λ_2 (hence $\tilde{\nu}_1$ and $\tilde{\nu}_2$) shift to λ_{1i} and λ_{2i} ($\tilde{\nu}_{1i}$ and $\tilde{\nu}_{2i}$), respectively, whereas the force constants k_1 and k_2 remain unchanged. For isotope substitution at the carbon atom, m_2 becomes m_{2i}, and M becomes $M_i^2 = m_1m_{2i}m_3/(m_1 + m_{2i} + m_3)$. The following expression may be derived:

$$\frac{\lambda_{1i}\lambda_{2i}}{\lambda_1\lambda_2} = \frac{\frac{1}{M_i^2} + \frac{\sin^2\theta}{m_{2i}^2}}{\frac{1}{M^2} + \frac{\sin^2\theta}{m_2^2}}$$

Upon rearrangement, we obtain

$$\sin^2\theta = \frac{1/M_i^2 - B/M^2}{B/m_2^2 - 1/m_{2i}^2}$$

where

$$B = \frac{\lambda_{1i}\lambda_{2i}}{\lambda_1\lambda_2} = \left(\frac{\tilde{\nu}_{1i}\tilde{\nu}_{2i}}{\tilde{\nu}_1\tilde{\nu}_2}\right)^2$$

For the present treatment, we use the data from ^{12}C^{16}O and ^{13}C^{16}O isotopes. Calibration of the equation against data from heme 5, where θ is assumed to be 180°, indicates that it is necessary to subtract 2 cm^{-1} from the observed $\tilde{\nu}_{1i}$ value. This is reasonable in view of the assumptions made. We choose to correct $\tilde{\nu}_{1i}$ instead of $\tilde{\nu}_{2i}$ because it is affected by the assumptions to a greater extent. We therefore suggest that the $\tilde{\nu}_{1i}$ values be corrected by this amount for all the heme–CO complexes. Thus, $B = [(\tilde{\nu}_{1i} - 2)\tilde{\nu}_{2i}/(\tilde{\nu}_1\tilde{\nu}_2)]^2$ has been used in our calculations.

It is of interest to note that the Fe–C–O angle in the FeSP-15 complex is smaller than that of FeSP-14 and FeSP-13 (Table I). The greater angle of bending (180° – θ) in FeSP-15 may be caused by the constraint imposed upon the oxygen atom rather than the carbon atom. As the hydrocarbon chain becomes shorter such as in the case of FeSP-14 and FeSP-13, the constraint is now imposed upon the carbon atom, resulting in a smaller "bend" but a greater "tilt". It is still not possible to quantitatively estimate the tilt angle from resonance Raman data. Nevertheless, we suggest that the tilt angle increases in the order FeSP-15 < FeSP-14 < FeSP-13, in parallel with the order of decreasing CO binding constants.

The increase in $\tilde{\nu}_1$(Fe–CO) from 495 cm^{-1} in heme 5 to 509 cm^{-1} in FeSP-15 may be caused primarily by the decrease in θ, which decreases the effective mass for the Fe–CO stretching vibration. Our normal coordinate analysis based on the model imidazole–Fe–C–O indicates that a change in the Fe–C–O angle from 180 to 167° *without changes in force constants* would increase the $\tilde{\nu}_1$(Fe–CO) frequency by ~23 cm^{-1}, which is larger than the 14 cm^{-1} observed here. The structural parameters used in our calculations are r(Fe–Im) = 2.10 Å, r(Fe–C) = 1.77 Å, r(C–O) = 1.12 Å, ϕ(Im–Fe–C) = 180°, and ϕ(Fe–C–O) = variable. The force constants (mdyn/Å) are K(Fe–Im) = 1.33, K(Fe–C) = 2.51, K(C–O) = 16.23, H(Im–Fe–C) = 0.57, and H(Fe–C–O) = 0.79. Stretching–stretching interaction force constants between two adjacent bonds are F[(Im–Fe)–(Fe–C)] = 0.10 mdyn/Å and F[(Fe–C)–(C–O)] = 1.20 mdyn/Å. Imidazole was treated as a single mass of 68 daltons. Other details may be found in Tsubaki et al. (1982). It is conceivable that the CO distortion caused by the steric interactions may decrease the Fe–C bond strength (hence the Fe–C stretching force constant), resulting in a smaller increase in $\tilde{\nu}_1$(Fe–CO). Also, the calculations show that the $\tilde{\nu}_2$(C–O) frequency should slightly increase (~2 cm^{-1}) by the CO distortion rather than decrease (from 1954 to 1945 cm^{-1}) as actually observed. Normally, a decrease in $\tilde{\nu}_2$(C–O) is associated with an increase of electron density in the antibonding CO (π^*) orbital.

The further increase in $\tilde{\nu}_1$(Fe–CO) to 512 (FeSP-14) and 514 cm^{-1} (FeSP-13) is interpreted as due to increased tilting,

which may enhance the interactions between the C atom of CO and the N atom(s) of the pyrrole ring(s). The distortion of the octahedral coordination about the iron can only weaken the Fe–C bond (hence increasing the Fe–C bond length). At present, there are no X-ray structural data from distorted heme–CO model complexes. However, all the Fe–C bond distances reported for carbonmonoxy hemoproteins (with distorted CO ligand) are greater than the 1.77-Å value found in FeTPP(Py)CO (Peng & Ibers, 1976). For example, a value of 1.80 Å has been given to the Fe–C bond length in HbA·CO (Baldwin, 1980). An even larger value of 2.4 Å was reported for carbonmonoxy erythrocruorin (Steigemann & Weber, 1979), although quantitatively its validity is doubtful. To account for the increase in the Fe–CO stretching frequency associated with CO tilting, the effect of C(CO)---N(pyrrole) interactions must be sufficiently large so that the force field provided by both Fe and pyrrole N for C motion is now greater than the force field previously provided by the Fe predominantly.

The tilting or bending of the CO ligand is likely to lower the CO (π^*) orbital energy and enhance its overlap with both the π and π^* orbitals of the porphyrin. In the ground state, the overlap facilitates the electron donation from a pyrrole ring to the CO ligand, which should increase the C(CO)---N(pyrrole) attraction (hence, vibrational couplings) and decrease the C–O bond order via increasing electron density in the CO (π^*) orbital. However, the CO tilting decreases the π-back-bonding through the iron, resulting in an increase in the CO bond order. The observed decrease in $\tilde{\nu}_2$(C–O) frequency with Fe–CO distortion (see Table I) may indicate that the former effect is greater than the latter.

Application of the present method to resonance Raman data of carbonmonoxy human hemoglobin A results in an ∠FeCO angle of 175 ± 5°, in good agreement with the linear Fe–C–O linkage assumed by Baldwin (1980) in her X-ray diffraction studies. Four subunits of HbA·CO complexes give rise to a single sharp $\tilde{\nu}_1$(Fe–CO) Raman line, indicating that the Fe–C–O geometry is nearly the same for all the subunits. On the other hand, our calculated ∠FeCO angle of 175 ± 5° for Mb·CO in solution differs considerably from the 135° value determined in crystals by neutron diffraction (Norvell et al., 1975). Significant differences between infrared spectra of crystals and solutions have been reported (Makinen et al., 1979). There are multiple Fe–CO conformers in Mb·CO as revealed by infrared (Makinen et al., 1979) and resonance Raman (Tsubaki et al., 1982) studies. The ∠FeCO angle (175 ± 5°) estimated here corresponds to the major conformer in Mb·CO, which gives rise to $\tilde{\nu}_1$(Fe–CO) and $\tilde{\nu}_2$(C–O) at 512 and 1944 cm^{-1}, respectively.

Enhancement of Fe–C–O Bending Vibration. The mechanism by which the Fe–C–O bending mode can be resonance enhanced via Soret excitation possibly resides in charge transfer from the porphyrin (π^*) to the CO (π^*) orbital. The electron density is high at the pyrrole nitrogens in the e_g (π^*) orbital; the charge transfer is facilitated by the increased orbital overlap caused by the CO tilting. It is conceivable that a significant electron population of the CO (π^*) orbital upon Soret excitation may cause the Fe–C–O linkage to bend in precisely the way caused by the Fe–C–O bending vibration. Thus, its intensity is thought to originate from Albrecht's *A* term or the Franck–Condon scattering mechanism (Felton & Yu, 1978).

We propose that the intensity of δ(Fe–C–O) relative to that of $\tilde{\nu}_1$(Fe–CO) is a measure of the overlap between porphyrin (π^*) and CO (π^*). The greater the steric hindrance, the greater the I_δ/I_ν value because of the increasing overlap caused by distortion (tilting). Further studies on sterically hindered hemes of known structure are needed for critically testing the hypothesis.

Intensity Variations Associated with Isotopic Substitution. We observed some striking changes in relative intensity at 504 and 512 cm^{-1} (Figure 4), which are caused by isotope substitution. The 512-cm^{-1} line assigned to the Fe–CO stretching mode of a distorted CO species appears to decrease its intensity relative to the 504-cm^{-1} line when $^{12}C^{16}O$ is replaced by $^{13}C^{16}O$, $^{12}C^{18}O$, or $^{13}C^{18}O$. There is no noticeable intensity decrease at 495 cm^{-1}, which has been assigned to the Fe–CO stretching vibration of a presumably linear and perpendicular Fe–C–O linkage. When there is a CO distortion, the $\tilde{\nu}$(Fe–C) and δ(Fe–C–O) coordinates are mixed to some extent. Upon isotope substitution, a normal mode that is predominantly Fe–CO stretching may change its projection on the geometry change associated with electronic excitation (L. Ziegler, G. Monteleone, and B. Hudson, personal communication), resulting in a change in its resonance Raman intensity (Felton & Yu, 1978). A large decrease has been observed in the resonance Raman intensity of amide III mode (predominantly N–H bending and C–N stretching) of *N*-methylacetamide upon deuterium substitution of the amide linkage (L. Ziegler, G. Monteleone, and B. Hudson, personal communication). When the Fe–C–O linkage is linear and perpendicular, the Fe–CO stretch does not mix with the bending mode so that the isotope substitution does not change its projection on the Fe–C bond. In fact, careful examination of the Fe–CO stretching mode at 512 cm^{-1} in Mb·CO [see Figure 6 of Tsubaki et al. (1982)] reveals some intensity decreases relative to the ring mode at 347 cm^{-1} when $^{12}C^{16}O$ is replaced by $^{13}C^{16}O$ or other heavier isotopes. Therefore, it may be tentatively concluded that the origin of the $\tilde{\nu}_1$(Fe–CO) intensity change by isotope substitution is the CO distortion, which induces vibrational mixing.

Acknowledgments

We thank Dr. B. Benko for discussions on three-body oscillator problems. Comments by Dr. D. L. Rousseau (Bell Laboratories) are greatly appreciated.

Registry No. Fe^{III} heme 5, 86550-09-6; Fe^{III}SP-13, 86550-10-9; Fe^{III}SP-14, 86550-11-0; Fe^{III}SP-15, 86550-12-1; Fe^{II}(heme 5)(N-MeIm)CO, 78778-39-9; Fe^{II}(SP-13)(N-MeIm)CO, 78789-48-7; Fe^{II}(SP-14)(N-MeIm)CO, 86550-13-2; Fe^{II}(SP-15)(N-MeIm)CO, 86550-14-3.

References

Alben, J. O., & Caughey, W. S. (1968) *Biochemistry 7*, 175–183.

Amstrong, R. S., Irwin, M. J., & Wright, P. E. (1982) *J. Am. Chem. Soc. 104*, 626–627.

Baldwin, J. M. (1980) *J. Mol. Biol. 136*, 103–128.

Barlow, C. H., Ohlsson, P.-I., & Paul, K.-G. (1976) *Biochemistry 15*, 2225–2229.

Callahan, P. M., & Babcock, G. T. (1981) *Biochemistry 20*, 952–958.

Caughey, W. S. (1970) *Ann. N.Y. Acad. Sci. 174*, 148–153.

Champion, P. M., Stallard, B. R., Wagner, G. C., & Gunsalus, I. C. (1982) *J. Am. Chem. Soc. 104*, 5469–5472.

Choi, S., Spiro, T. G., Langry, K. C., Smith, K. M., Budd, D. L., & LaMar, G. N. (1982) *J. Am. Chem. Soc. 104*, 4345–4351.

Collman, J. P., Gagne, R. R., Reed, C. A., Robinson, W. T., & Rodley, G. A. (1974) *Proc. Natl. Acad. Sci. U.S.A. 71*, 1326–1329.

Collman, J. P., Brauman, J. I., Halbert, T. R., & Suslick, K. S. (1976) *Proc. Natl. Acad. Sci. U.S.A. 73*, 3333–3337.
Collman, J. P., Brauman, J. I., & Doxsee, K. M. (1979) *Proc. Natl. Acad. Sci. U.S.A. 76*, 6035–6039.
Felton, R. H., & Yu, N.-T. (1978) in *The Porphyrins* (Dolphin, D., Ed.) Vol. 3, pp 347–393, Academic Press, New York.
Heidner, E. J., Ladner, R. C., & Perutz, M. F. (1976) *J. Mol. Biol. 104*, 707–722.
Hoard, J. L. (1975) in *Porphyrins and Metalloporphyrins* (Smith, K. M., Ed.) p 351, Elsevier, New York.
Huber, R., Epp, O., & Formanek, H. (1970) *J. Mol. Biol. 52*, 349–354.
Kerr, E. A., Mackin, H. C., & Yu, N.-T. (1982) *Biophys. J. 37*, 371a.
Kerr, E. A., Mackin, H. C., & Yu, N.-T. (1983) *Biochemistry* (in press).
Kim, J. B., Adler, A. D., & Longo, F. R. (1978) in *The Porphyrins* (Dolphin, D., Ed.) Vol. 1, Chapter III, Academic Press, New York.
Kroeker, R. M., Hansma, P. K., & Kaska, W. C. (1980) *J. Chem. Phys. 72*, 4845–4852.
Mackin, H. C., Tsubaki, M., & Yu, N.-T. (1983) *Biophys. J. 41*, 349–357.
Makinen, M. W., Houtchens, R. A., & Caughey, W. S. (1979) *Proc. Natl. Acad. Sci. U.S.A. 76*, 6042–6046.
Moffat, K., Deatherage, J. F., & Seybert, D. W. (1970) *Science (Washington, D.C.) 206*, 1035–1042.
Norvell, J. C., Nunes, A. C., & Schoenborn, B. P. (1975) *Science (Washington, D.C.) 190*, 568–570.
Padlan, E. A., & Love, W. E. (1975) *J. Biol. Chem. 249*, 4067–4078.
Peng, S. M., & Ibers, J. A. (1976) *J. Am. Chem. Soc. 98*, 8032–8036.
Perutz, M. F. (1976) *Br. Med. Bull. 32*, 195–208.
Phillips, S. E. V. (1978) *Nature (London) 273*, 247–248.
Phillips, S. E. V. (1980) *J. Mol. Biol. 142*, 531–554.
Rousseau, D. L., & Ondrias, M. R. (1983) *Annu. Rev. Biophys. Bioeng.* (in press).
Rousseau, D. L., Ondrias, M. R., LaMar, G. N., Kong, S. B., & Smith, K. M. (1983) *J. Biol. Chem. 258*, 1740–1746.
Shaanan, B. (1982) *Nature (London) 296*, 683–684.
Spaulding, L. D., Chang, C. C., Yu, N.-T., & Felton, R. H. (1975) *J. Am. Chem. Soc. 97*, 2517–2525.
Spiro, T. G., Stong, J. D., & Stein, P. (1979) *J. Am. Chem. Soc. 101*, 2648–2655.
Steigemann, W., & Weber, E. (1979) *J. Mol. Biol. 127*, 309–338.
Szabo, A. (1978) *Proc. Natl. Acad. Sci. U.S.A. 75*, 2108–2111.
Traylor, T. G. (1981) *Acc. Chem. Res. 14*, 102–109.
Tsubaki, M., Srivastava, R. B., & Yu, N.-T. (1982) *Biochemistry 21*, 1132–1140.
Ward, B., Wang, C.-B., & Chang, C. K. (1981) *J. Am. Chem. Soc. 103*, 5236–5238.
Wilson, E. (1939) *J. Chem. Phys. 7*, 1047–1052.
Yu, N.-T., & Srivastava, R. B. (1981) *J. Raman Spectrosc. 9*, 166–171.

Differentiation of Enzyme and Substrate Binding in the Prothrombinase Complex†

Marjorie M. Tucker, Michael E. Nesheim, and Kenneth G. Mann*

ABSTRACT: The Ca^{2+} dependence of factor Xa binding to phospholipid vesicles was measured in the presence and absence of factor Va. The increase in polarization of a fluorescently labeled derivative of factor Xa, [5-(dimethylamino)-1-naphthalenesulfonyl]glutamylglycylarginyl factor Xa (Dns-EGR-Xa), was used as a probe to measure the interaction of factor Xa with phospholipid. The Ca^{2+} concentration required for half-maximal binding of Dns-EGR-Xa to phospholipid vesicles was 3.5×10^{-4} M in the presence of factor Va and 9.5×10^{-4} M in the absence of factor Va. At a Ca^{2+} concentration of 5×10^{-4} M, the binding of Dns-EGR-Xa to phospholipid-bound factor Va was near maximal, whereas there was no detectable interaction of Dns-EGR-Xa with phospholipid alone at this Ca^{2+} concentration as detected by fluorescence polarization. These results were qualitatively confirmed by high-performance liquid chromatography. The rate of hydrolysis of the factor Xa synthetic substrate, benzoylisoleucylglutamylglycylarginine *p*-nitroanilide, by factor Xa in the presence of factor Va and phospholipid decreased in a Ca^{2+}-dependent manner. These data were analyzed as fraction of factor Xa bound to the phospholipid. A Ca^{2+} concentration of 2.7×10^{-4} M resulted in half-maximal binding by this technique. The relationship observed between rates of prothrombin activation and Ca^{2+} concentration could be predicted quantitatively from calculations of local enzyme and substrate concentrations.

The maximum rate of conversion of prothrombin to thrombin by factor Xa requires factor Va, phospholipid, and Ca^{2+} ions. The activity is dependent on the condensation of substrate (prothrombin), enzyme (factor Xa), and cofactor (factor Va) on the surface of the phospholipid. The integrity of this prothrombinase complex is dependent on Ca^{2+} ions, as was initially shown by Papahadjopoulos & Hanahan (1964). The binding of prothrombin to phospholipid is also dependent on Ca^{2+} ions (Nelsestuen et al., 1976; Nelsestuen & Lim, 1977; Prendergast & Mann, 1977; Nelsestuen & Broderius, 1977; Lim et al., 1977; Dombrose et al., 1979). The binding of the vitamin K dependent proteins to phospholipid is thought to

† From the Hematology Research Section, Mayo Clinic/Foundation, Rochester, Minnesota 55905. *Received December 3, 1982.* Supported by National Institutes of Health Grants HL-16150, HL-17430, HL-26070, and HL-27076 from the National Heart, Lung, and Blood Institute and by the Mayo Foundation.

0006-2960/83/0422-4540$01.50/0